J. Fluid Mech. (1989), *vol.* 209, *pp.* 285–308
Printed in Great Britain

A numerical study of the interaction between unsteady free-stream disturbances and localized variations in surface geometry

By R. J. BODONYI[1], W. J. C. WELCH[2], P. W. DUCK[2] AND M. TADJFAR[1]

[1] Department of Aeronautical & Astronautical Engineering, The Ohio State University, 2036 Neil Ave. Mall, Columbus, OH 43210, USA

[2] Department of Mathematics, University of Manchester, Manchester M13 9PL, UK

(Received 29 August 1988 and in revised form 1 May 1989)

A numerical study of the generation of Tollmien–Schlichting (T–S) waves due to the interaction between a small free-stream disturbance and a small localized variation of the surface geometry has been carried out using both finite-difference and spectral methods. The nonlinear steady flow is of the viscous–inviscid interactive type while the unsteady disturbed flow is assumed to be governed by the Navier–Stokes equations linearized about this flow. Numerical solutions illustrate the growth or decay of the T–S waves generated by the interaction between the free-stream disturbance and the surface distortion, depending on the value of the scaled Strouhal number. An important result of this receptivity problem is the numerical determination of the amplitude of the T–S waves.

1. Introduction

The steady and unsteady effects of small surface-mounted obstacles on the boundary-layer flow over a surface have been of concern for many years. These effects include most notably separation and instability, often leading to transition to turbulence. Two main possible reasons for this transition have been suggested: either the surface distortion produces, in effect, a locally separated shear flow which is susceptible to inviscid instabilities associated with the inflectional velocity profile (see Smith & Bodonyi 1982, 1985, 1987 and Bodonyi, Smith & Gajjar 1983 for a discussion of these inviscid-type instabilities), or there is a sensitive interaction between the surface distortion and the basic flow, possibly with unsteadiness/turbulence in the free stream, which can readily accentuate the viscous–inviscid growth of the Tollmien–Schlichting instabilities usually present in boundary layers in any case.

The major steady-flow phenomenon observed, separation, is now well understood, at least in two-dimensional flows. It is generally of an interactive viscous–inviscid type in which the flows inside and outside the boundary layer affect each other significantly within a relatively short lengthscale. The question of the stability of the separating flow or other locally distorted steady or unsteady motions is always present, however, and this has started to receive increased attention, in part because of modern developments in boundary-layer methods.

In this study our concern is with the possibility of the generation of Tollmien–Schlichting (T–S) waves due to the interaction of small free-stream

disturbances and localized variations in the surface geometry. In general terms, the sequence of events that begins with the excitation of spatially growing T–S waves in a boundary layer by free-stream disturbances is known as the receptivity problem (Morkovin 1969). It has been studied by a number of authors over the years and the area has been reviewed by Reshotko (1976). More recently, Murdock (1980), Goldstein (1983, 1984, 1985), Goldstein, Sockol & Sanz (1983) and Goldstein, Leib & Cowley (1987) have theoretically investigated the role that small free-stream disturbances play in generating T–S waves in boundary-layer flows in a variety of situations. In particular we note that Goldstein (1985) studied the effect that small variations in surface geometry have on scattering weak unsteady free-stream disturbances into T–S waves. Using the triple-deck scalings of Stewartson (1969), Goldstein concluded that relatively small surface variations which provoke correspondingly small pressure changes can produce a large coupling between the T–S waves and the imposed disturbance when these variations are sufficiently rapid, i.e. when they occur on the scale of a T–S wave. Goldstein's analysis provided a qualitative explanation of the Leehey & Shapiro (1979) boundary-layer receptivity measurements. Further comparisons with the Leehey & Shapiro experiments using a solution of the local Orr–Sommerfeld equation have been made by Goldstein & Hultgren (1987).

However, Goldstein's analysis is limited in that he took for the steady flow the linearized solution of Stewartson (1970, 1971) for the interactive flow in the vicinity of a sharp corner in an incompressible flow. Thus Goldstein could not consider the effects of surface variations of sufficient size to provoke boundary-layer separation or even a nonlinear response in the steady flow, although his analysis does account for non-parallel flow effects on the stability of the flow.

Since our interest is in the stability of non-parallel flows and especially those with strong local streamwise variations in surface geometry, it is appropriate to take the steady nonlinear viscous–inviscid interactive solutions, of the triple-deck and similar kinds, for the basic steady motion. This is because, as is now well known, flow reversal for small- or large-scale separations occurring in such flows is not necessarily a catastrophic event: the solution at the separation point is regular owing to the presence of interaction, unlike that in steady classical, i.e. non-interactive, boundary layers for instance. Hence a steady non-parallel basic flow with a small localized region of reversed flow can be described fully by the classical boundary-layer equations, subject to an unknown pressure which must also be computed as part of the solution. Additionally, we shall assume that the unsteady flow is governed by the linearized Navier–Stokes equations, as discussed in the following section.

2. Problem formulation

We wish to study the interaction between an unsteady free-stream and a small surface perturbation on a flat plate, such as a hump or trough, for an incompressible two-dimensional viscous flow. Thus following Goldstein (1985) we take the upstream motion to consist of a uniform flow with velocity U_∞^* plus a small harmonic perturbation of frequency Ω and constant amplitude $u_\infty^* \ll U_\infty^*$, so that the unsteady motion can be analysed as a linear perturbation of the uniform steady flow, U_∞^*, i.e. $U_\infty^*(1 + u_\infty^*/U_\infty^* \, \mathrm{e}^{-\mathrm{i}\Omega t^*})$.

Consider a Cartesian coordinate system (x^*, y^*) with x^* tangent to and y^* normal to the flat plate with the origin taken at the leading edge. Further, define the Reynolds number $Re = U_\infty^* L^*/\nu$, where L^* is the distance of the surface perturbation

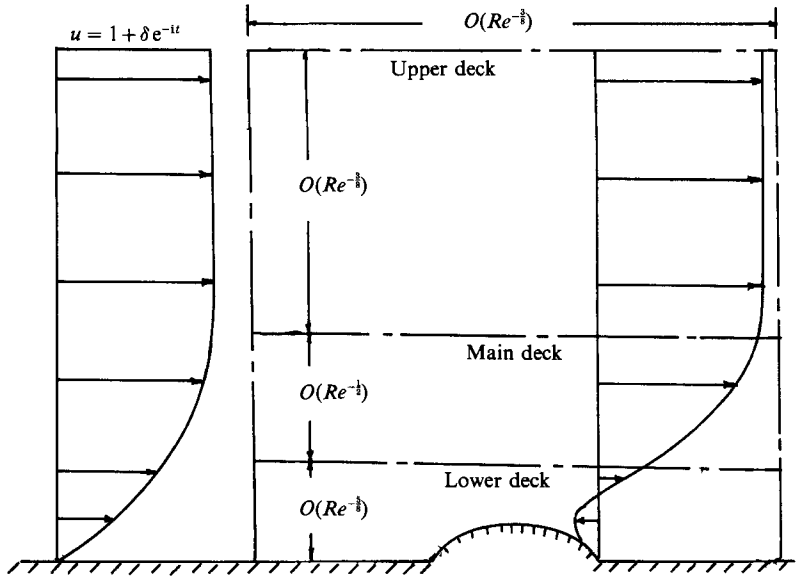

FIGURE 1. Schematic of the triple-deck flow structure.

from the leading edge of the flat plate and ν is the kinematic viscosity of the fluid. For convenience, we introduce the small parameter $\epsilon = Re^{-\frac{1}{8}}$ and consider solutions of the Navier–Stokes equations when $Re \gg 1$. Specifically, we wish to consider the problem of flow over a small hump of length $O(L^*\epsilon^3)$ and height $O(L^*\epsilon^5)$ with a profile of the form

$$\frac{y^*}{L^*} = \epsilon^5 F\left(\frac{x^*-L^*}{\epsilon^3 L^*}\right), \tag{2.1}$$

with $F = O(1)$, positioned at a distance L^* from the leading edge. The interaction region is shown schematically in figure 1.

Following Goldstein (1985) we write

$$\hat{U}(x,y,t) = U_0(x,y) + \delta\tilde{u}(x,y,t), \tag{2.2}$$

$$\hat{V}(x,y,t) = V_0(x,y) + \delta\tilde{v}(x,y,t), \tag{2.3}$$

$$\hat{P}(x,y,t) = P_0(x,y) + \delta\tilde{p}(x,y,t), \tag{2.4}$$

where the steady velocity components U_0, V_0, and pressure P_0, are normalized by U^*_∞ and ρU^{*2}_∞ respectively and $\tilde{u}, \tilde{v}, \tilde{p}$, the unsteady velocity and pressure terms, normalized by u^*_∞ and $\rho u^*_\infty U^*_\infty$, respectively. Furthermore, we define

$$x = \frac{x^*-L^*}{L^*}, \quad y = \frac{y^*}{L^*}, \quad t = \Omega t^*, \quad \delta = \frac{u^*_\infty}{U^*_\infty}. \tag{2.5}$$

Substituting (2.2)–(2.4) into the Navier–Stokes equations and neglecting terms of $O(\delta^2)$, we get the linearized perturbation equations

$$S\tilde{u}_t + U_0\tilde{u}_x + \tilde{u}U_{0x} + V_0\tilde{u}_y + \tilde{v}U_{0y} = -\tilde{p}_x + Re^{-1}[\tilde{u}_{xx} + \tilde{u}_{yy}], \tag{2.6}$$

$$S\tilde{v}_t + U_0\tilde{v}_x + \tilde{u}V_{0x} + V_0\tilde{v}_y + \tilde{v}V_{0y} = -\tilde{p}_y + Re^{-1}[\tilde{v}_{xx} + \tilde{v}_{yy}], \tag{2.7}$$

$$\tilde{u}_x + \tilde{v}_y = 0, \tag{2.8}$$

where $$S = \Omega L^*/U_\infty^*, \tag{2.9}$$

is the Strouhal number.

Finally, we note that the physical interaction between the oncoming boundary layer, free-stream disturbance, and hump is governed by a triple-deck structure, centred near the surface distortion. The details of the structure as applied to this problem have been given by Goldstein (1985) and we, therefore, only summarize the relevant portions here. As is usually the case the viscous interaction problem essentially reduces to a study of the lower-deck equations. Thus the appropriately scaled variables in the lower deck for the steady flow are

$$U_0(x, y) = \epsilon U(X, Y) + O(\epsilon^2), \tag{2.10}$$

$$V_0(x, y) = \epsilon^3 V(X, Y) + O(\epsilon^4), \tag{2.11}$$

$$P_0(x, y) = \epsilon^2 P(X) + O(\epsilon^3), \tag{2.12}$$

where $$X = x/\epsilon^3, \quad Y = y/\epsilon^5. \tag{2.13}$$

U, V, and P are found from the solution of the lower-deck equations:

$$U_X + V_Y = 0, \tag{2.14}$$

$$UU_X + VU_Y = -P_x + U_{YY}, \tag{2.15}$$

subject to the boundary conditions

$$U = V = 0 \quad \text{on} \quad Y = F(X), \tag{2.16}$$

$$(U, V, P) \to (Y, 0, 0) \quad \text{as} \quad |X| \to \infty, \tag{2.17}$$

$$U \to [Y + A(X)], \quad Y \to \infty, \quad \text{all} \quad X, \tag{2.18}$$

where we have assumed that a simple renormalization of the variables has been carried out in order to set the value of the wall shear of the oncoming, undisturbed boundary layer to unity. Finally, the interaction condition for incompressible flow is given by the Cauchy Hilbert integral

$$P(X) = \frac{1}{\pi} \int_{-\infty}^{\infty} (X - \xi)^{-1} \frac{\mathrm{d}A}{\mathrm{d}\xi} \mathrm{d}\xi. \tag{2.19}$$

This steady problem was originally formulated by Smith (1973).

For the unsteady flow we introduce the following lower-deck variables:

$$\tilde{u}(x, y, t) = \mathrm{e}^{-\mathrm{i}t} u(X, Y) + O(\epsilon), \tag{2.20}$$

$$\tilde{v}(x, y, t) = \epsilon^2 \mathrm{e}^{-\mathrm{i}t} v(X, Y) + O(\epsilon^3), \tag{2.21}$$

$$\tilde{p}(x, y, t) = \epsilon \mathrm{e}^{-\mathrm{i}t} p(X) + O(\epsilon^2). \tag{2.22}$$

In these expressions we have utilized the fact that since the unsteady flow is governed by the linearized Navier–Stokes equations we can seek solutions which have a harmonic time dependence. Substituting (2.13), (2.20)–(2.22) into (2.6)–(2.8) yields, to leading order in ϵ,

$$-\mathrm{i}\epsilon^2 S u + U u_X + u U_X + V u_Y + v U_Y = -p_X + u_{YY}, \tag{2.23}$$

$$u_X + v_Y = 0. \tag{2.24}$$

As noted in §1, our interest in this paper is in the relatively high-frequency case where we choose Ω to be of the same order as the T–S wave frequency at and

upstream of the lower branch of the neutral stability curve. For this reason we require that $\Omega = O(\epsilon^{-2})$, i.e. the Strouhal number $S = O(\epsilon^{-2})$. Thus we define a scaled Strouhal number S_0 such that

$$S_0 = \epsilon^2 S, \quad S_0 = O(1). \tag{2.25}$$

Furthermore, in this case the Stokes-layer thickness is found to be of $O(\epsilon)$ also and, therefore, it will be of $O(\epsilon^5)$ in terms of the lower-deck scalings. Hence the Stokes-layer thickness is the same as that of the lower deck. Upstream of the triple-deck region, where the mean flow changes on the scale of x, the unsteady flow in the boundary layer is given by the Stokes solution, which can be written in terms of the lower-deck scalings, as

$$u = 1 - \exp(\mathrm{i}^{\frac{3}{2}} S_0^{\frac{1}{2}} Y), \tag{2.26}$$

$$p = \mathrm{i} X S_0. \tag{2.27}$$

The lower-deck problem is completed by solving (2.23), (2.24) using (2.25) subject to the no-slip condition at the wall

$$u = v = 0 \quad \text{on} \quad Y = F(X), \tag{2.28}$$

matching with the main-deck solution

$$u \to 1 + a(X), \quad Y \to \infty, \quad \text{all} \quad X, \tag{2.29}$$

and matching with the upstream Stokes-layer solution given by (2.26) and (2.27) for $X \to -\infty$. Finally, the relationship between $a(X)$ and $\mathrm{d}p/\mathrm{d}X$ is given by the interaction condition

$$\frac{\mathrm{d}^2 a}{\mathrm{d}X^2} = \frac{1}{\pi} \int_{-\infty}^{\infty} \frac{\mathrm{d}p/\mathrm{d}\xi - \mathrm{i}S_0}{(\xi - X)} \mathrm{d}\xi. \tag{2.30}$$

It was found that numerical solutions of the disturbance equations were not obtainable for supercritical disturbances using the interaction law (2.30). Thus an alternative method used by Bodonyi & Duck (1988) in treating three-dimensional interacting flows has been employed here. In this approach, the relationship between the pressure $p(X)$ and displacement thickness $-a(X)$ is found through a numerical solution of the upper-deck equations as opposed to the Hilbert integral representation (2.30). Specifically, it can be shown that the appropriate boundary-value problem in the upper deck for the disturbance pressure is given by

$$\hat{p}_{XX} + \hat{p}_{\hat{y}\hat{y}} = 0, \tag{2.31}$$

with boundary conditions

$$\hat{p}_{\hat{y}}(X, 0) = \frac{\mathrm{d}^2 a}{\mathrm{d}X^2}, \tag{2.32}$$

$$\hat{p}(X, \hat{y}) \to 0, \quad \hat{y} \to \infty, \quad \text{all} \quad X, \tag{2.33}$$

$$\hat{p}(X, \hat{y}) + \mathrm{i}S_0 X \to p(X) \quad \text{as} \quad \hat{y} \to 0, \tag{2.34}$$

$$\hat{p} \to 0 \quad \text{as} \quad X \to -\infty, \tag{2.35}$$

$$\hat{p}_X - \mathrm{i}k\hat{p} \to 0 \quad \text{as} \quad X \to \infty, \tag{2.36}$$

where we have written

$$p - p_\infty = \epsilon[\hat{p}(X, \hat{y}) + \mathrm{i}S_0 X], \quad \hat{y} = y/\epsilon^3. \tag{2.37}$$

Note that (2.36) defines a radiation condition applied on the disturbance pressure at the downstream boundary to simulate the outward-propagating pressure disturbances there. The wavenumber k, which depends on S_0, is found from the solution of the classical Orr–Sommerfeld eigenvalue problem for the Stokes-layer flow. Alternatively, k can be computed iteratively from the numerical computations, as will be discussed below.

The entire unsteady solution is thus known once the solution of this boundary-value problem has been obtained. As a special case Goldstein (1985) gives an analytical solution to the problem using a linearized solution of the steady-flow problem for a slightly cranked flap on a flat plate due to Stewartson (1970, 1971). Utilizing these results for $U(X, Y)$, $V(X, Y)$ and $P(X)$ Goldstein was able to solve the unsteady problem using a Fourier transform technique.

In this paper we solve the corresponding problem for surface distortions such that the steady flow is fully nonlinear in character. However, in this case both the steady and the unsteady problems must be solved numerically. Before discussing the numerical approaches used in this study it is appropriate to note that the problem formulated above differs in a significant way from the usual hydrodynamic stability problem which generally involves the solution of the Orr–Sommerfeld equation. The Orr–Sommerfeld eigenvalue problem when applied to boundary-layer flows leads to the solution for 'free' disturbances which are, in fact, the normal modes of the boundary layer and they are usually referred to as the Tollmien–Schlichting waves. While important in their own right, the normal mode representation of a small-disturbance spectrum cannot be conveniently extended to finite-amplitude, i.e. nonlinear disturbances, nor are they useful by themselves in understanding how external disturbances, such as free-stream turbulence or surface roughness, etc, feed energy into the boundary layer, thereby exciting spatially growing T–S waves.

One approach to understanding both the linear and nonlinear evolution of T–S waves in a boundary layer is to consider an initial-value problem, using the unsteady triple-deck equations. Such studies have been carried out recently by Smith (1985), Smith & Burggraf (1985), and Duck (1985).

Alternatively, one can study the nature of the coupling between an imposed free-stream disturbance and the growth of T–S waves in the boundary layer. This receptivity problem differs from the hydrodynamic stability problem both physically and mathematically. Physically, it is the response in the boundary layer to some externally imposed disturbance. Mathematically, it is no longer an eigenvalue problem. Instead it is a boundary-value problem as can be seen from (2.23)–(2.24) and (2.26)–(2.30), wherein the boundary layer is driven by some external forced oscillation with its response being a solution of the linearized disturbance equations having the same frequency and phase speed as the particular forcing disturbance being studied. The primary objective of this work is a detailed numerical study of this receptivity problem for a range of values of S_0, which represents the nature of the free-stream disturbance, and a representative surface distortion which we take to be

$$F(X) = h(1+X^2)^{-1}, \tag{2.38}$$

where h is an order-one factor which gives the height of the distortion relative to the lower-deck scalings.

3. Numerical method

3.1. *Steady-state solution*

First we consider the steady-flow problem defined by (2.14)–(2.19) along with (2.38). Numerical solutions have been found using a finite-difference procedure developed by Smith & Bodonyi (1985). Briefly, the governing equations are replaced by difference representations for ψ, $U = \psi_Y$, $\tau = U_Y$, and P with uniform steps in X, Y. The computational domain extends from $X = X_1 (< 0)$ to $X = X_2 (> 0)$ and from $Y = 0$ to $Y = Y_\infty$, with starting conditions (2.17) specified, in effect, at $X = X_1$.

The nonlinear difference equations at a given streamwise location X are solved to within a tolerance of 10^{-6} in absolute value by Newtonian iteration using Gaussian elimination and back substitution. The solution is then advanced to the next streamwise location and the process repeated until the entire domain is covered. Since the problem is interactive, multiple forward-marching sweeps are necessary until a tolerance of 10^{-5} between successive values obtained for $P(X)$ is satisfied for all X. At this point the solution is said to have converged in the global sense. The diagonally dominant nature of the finite-difference form of the interaction law (2.19) makes this multi-sweeping process both fast and stable. Whenever flow reversal occurs, i.e. $U < 0$, windward differencing is used to represent UU_X in finite-difference form.

The numerical solution has been found using (2.38) for the surface shape with $h = 0.1$, 1.0 and 5.0. Representative distributions of the wall shear $\tau(X, 0)$, and pressure, $P(X)$, of the steady flow are given in figure 2 for $h = 5.0$.

With the steady solution known, we now proceed to consider the numerical solution of the complex unsteady linearized boundary-layer equations (2.23) and (2.24). Two approaches have been used to solve the disturbance equations. In the first approach, the equations were solved in the physical plane using a finite-difference method, while in the second a spectral numerical scheme was used. Reasons for considering both approaches are given later. First we describe the methods.

3.2. *Unsteady solution – finite-difference method*

In this approach equations (2.23) and (2.24) were replaced, after subtracting out the Stokes shear-wave solution, by a system of difference equations of second-order accuracy to be consistent with the numerical method used for the steady-flow problem. Since the governing equations are linear no iteration in the normal direction is necessary at a fixed streamwise location. A single sweep across the boundary-layer region was sufficient to determine the solution there. Thus one complete sweep of the computational domain could be accomplished quickly. Multiple sweeps of the entire domain are still necessary to obtain the global solution, however, owing to the elliptic nature of the interaction law (2.30) or (2.31)–(2.36).

Initial attempts to solve the problem were made using the pressure-displacement interaction law (2.30) in a form utilizing the ideas first put forward by Veldman (1979) and fully discussed by Smith & Bodonyi (1985). Indeed, for values of $S_0 \leqslant 1$ acceptable solutions could be found. However, as the scaled frequency S_0 was increased towards its critical (i.e. neutral) value of $S_{0_{\text{crit}}} \approx 2.296$ acceptable numerical solutions became increasingly more difficult to obtain. It appears that these difficulties are related to the use of the interaction condition (2.30). Numerically, the Hilbert integral is truncated to the finite range $X_1 \leqslant \xi \leqslant X_2$, thus it is implicitly assumed that the tails of the integral over $-\infty < \xi < X_1$ and $\xi > X_2$ are negligibly

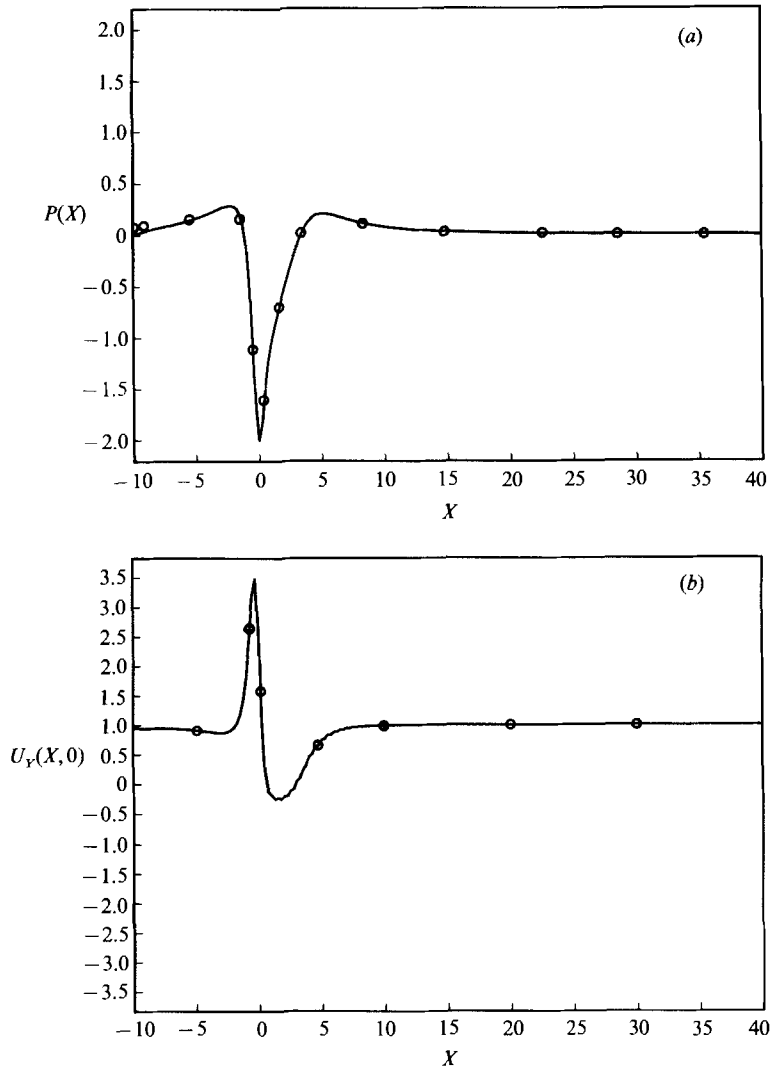

FIGURE 2. (*a*) Pressure distribution for steady flow, (*b*) wall shear distribution for steady flow, with $h = 5$. ——, finite-difference method; ○, spectral method.

small. This assumption appears to be satisfactory for the upstream 'tail', but it is questionable for the downstream behaviour of the integral. Furthermore, in addition to the difficulties associated with the finite integration domain, there is some question as to the convergence properties of the Cauchy–Hilbert integral itself, at least when the disturbances are supercritical, owing to the exponentially growing form of the disturbance quantities downstream.

To overcome these difficulties, the method developed by Bodonyi & Duck (1988) for solving flows with viscous–inviscid interaction has been successfully applied to this problem. In this method the relationship between the disturbance pressure and displacement thickness is found through a numerical solution of the appropriate upper-deck equations (2.31)–(2.36) as opposed to the Hilbert integral representation of the solution, (2.30). The crucial feature of the scheme is the inherent numerical

coupling between the viscous boundary-layer solution and the inviscid outer-flow solution which is carried out simultaneously in the spirit of the scheme proposed by Veldman (1979). Using this approach, the difficulties associated with the convergence of the Hilbert integral for supercritical disturbances can be avoided and the proper downstream boundary condition (radiation condition, see (2.36)) can be applied to the disturbance pressure.

For numerical convenience we apply the Prandtl transposition law and we also subtract out the Stokes solution. Thus consider the following change of variables:

$$u(X,Y) = 1-\exp(\mathrm{i}^{\frac{3}{2}}S_0^{\frac{1}{2}}Y)+u_0(X,Y), \tag{3.1}$$

$$v(X,Y) = v_0(X,Y), \quad \frac{\mathrm{d}p}{\mathrm{d}X}-\mathrm{i}S_0 = \frac{\mathrm{d}p_0}{\mathrm{d}X}. \tag{3.2}$$

Then the disturbance equations can be written as

$$u_{0X}+v_{0Y} = 0, \tag{3.3}$$

$$(U_X-\mathrm{i}S_0)\,u_0+Uu_{0X}+U_Y v_0+Vu_{0Y}+\frac{\mathrm{d}p_0}{\mathrm{d}X}-u_{0YY}$$
$$= -U_X+[U_X+\mathrm{i}^{\frac{3}{2}}S_0^{\frac{1}{2}}V]\exp(\mathrm{i}^{\frac{3}{2}}S_0^{\frac{1}{2}}Y), \tag{3.4}$$

with boundary conditions

$$u_0 = v_0 = 0 \quad \text{on} \quad Y = 0, \quad \text{all} \quad X, \tag{3.5}$$

$$u_0 \to 0 \quad \text{as} \quad X \to -\infty, \quad \text{all } Y, \tag{3.6}$$

$$u_0 \sim a(X)+\exp(\mathrm{i}^{\frac{3}{2}}S_0^{\frac{1}{2}}Y) \quad \text{as} \quad Y \to \infty, \quad \text{all} \quad X. \tag{3.7}$$

Given a guess or an update for u_0, v_0, $p_0(X)$ and $\hat{p}(X,\hat{y})$ everywhere, (3.3)–(3.7) are marched forward in X, while simultaneously (2.31)–(2.36) are solved along a line of varying $\hat{y}$. This then determines the complex-valued functions u_0, v_0, p and $\hat{p}$ (and hence $a(X)$) at a given streamwise location X. Sweeping through all X stations constitutes one global iteration. Convergence is finally attained when a global convergence test on the disturbance displacement thickness $-a(X)$ is satisfied.

The main features of the numerical scheme are the following. Two- and three-point differencing in Y is used for (3.3) and (3.4) respectively, with (3.7) applied at $Y = Y_\infty$. Three-point central differencing is used to approximate (2.31) in both dimensions, while condition (2.33) is applied at $\hat{y} = \hat{y}_\infty$. Equation (2.32) is approximated by one-sided differencing in $\hat{y}$ and a second-order scheme for X-derivatives. Finally, the radiation condition is applied in the following form to estimate the disturbance pressure at the downstream boundary

$$\hat{p}(X_{\max},\hat{y}) = \frac{\hat{p}(X_{\max}-2\Delta X,\hat{y})-4\hat{p}(X_{\max}-\Delta X,\hat{y})}{2\mathrm{i}k\Delta X-3}.$$

The value for k is either prescribed as discussed earlier, or by estimating its value from the relation $(\partial\hat{p}/\partial X)/\mathrm{i}\hat{p}$ from values of X reasonably far downstream, and then feeding this value back into the numerical computations. Numerically, the results indicate only slight differences in estimating k in these two ways. This is not very surprising since the viscous–inviscid interaction is a local phenomenon and the behaviour far downstream should approach that of the classical stability theory.

Supposing we have n points in Y and m points in $\hat{y}$, then at each X station, the difference approximation of (3.3), (3.4) and (2.31), together with the interface

conditions (2.34) and (3.7) can be written conveniently in matrix form as discussed by Bodonyi & Duck (1988). The overall scheme is nominally second-order accurate in the grid spacings ΔX, ΔY and $\Delta\hat{y}$. The resulting matrix equation is then solved using standard Gaussian elimination procedures and back substitution. Before discussing the numerical results we present the spectral method for solving the governing equations.

3.3. *Unsteady solution – spectral methods*

The spectral scheme described in this section was first developed for the computation of steady two-dimensional triple-deck flows (Burggraf & Duck 1981; Duck 1984). Later it was used to solve unsteady triple-deck flows by Duck (1985, 1988) and extended to solve three-dimensional steady and unsteady problems by Duck & Burggraf (1986) and Duck (1989). As explained in Duck (1985), the advantages of this scheme over more conventional finite-difference methods are first that it is easy to treat diverse interaction laws; secondly that flow reversal is handled correctly without the need for any special treatment; thirdly that it can easily be extended to solve three-dimensional flows; and fourthly, the so-called linearized flows (corresponding to $h \to 0$) may be solved without iteration.

In this paper we apply the spectral method to the disturbance equations. We replace (2.20)–(2.22) with

$$\left.\begin{aligned} &\tilde{u}(x,y,t) = u(X,Y,t)+O(\epsilon), \quad \tilde{v}(x,y,t) = \epsilon^2 v(X,Y,t)+O(\epsilon^3),\\ &\tilde{p}(x,y,t) = \epsilon p(X,t)+O(\epsilon^2), \end{aligned}\right\} \tag{3.8}$$

then write $u = \tilde{u}_0 + \tilde{u}$, where $\tilde{u}_0$ is the Stokes solution and $\tilde{u}$ is the unsteady perturbation to the Stokes solution. We introduce the new variable $\tilde{\tau} = \tilde{u}_y$ and transform (2.23) (with the time derivative restored) from physical space to wavenumber space, using (2.10)–(2.13), by taking the Fourier transform in the X-direction giving

$$S_0 \tilde{\tau}_t^* + \mathrm{i}kY\tilde{\tau}^* - \tau_{YY}^* = -R_1^* - R_2^*, \tag{3.9}$$

where

$$\tilde{\tau}^* = \int_{-\infty}^{\infty} \tilde{\tau}(X,Y,t)\,\mathrm{e}^{-\mathrm{i}kX}\,\mathrm{d}X,$$

and similarly for the other variables. For numerical reasons, it is convenient to map the Y-coordinate onto the η-coordinate where $Y = f(\eta)$ so that $0 \leqslant Y < \infty$ is mapped onto $0 \leqslant \eta \leqslant 1$ say. A uniform grid in η is chosen and with a suitable choice of $f(\eta)$ this corresponds to a non-uniform grid in Y-space concentrated near $Y = 0$. We choose $f(\eta) = \eta/(1-\eta)$. Then (3.9) becomes

$$S_0 \tilde{\tau}_t^* + \mathrm{i}kf(\eta)\,\tilde{\tau}^* - \frac{\tilde{\tau}_{\eta\eta}^*}{\{f'(\eta)\}^2} + \frac{\tilde{\tau}_\eta f''(\eta)}{\{f'(\eta)\}^3} = -R_1^* - R_2^* \tag{3.10a}$$

with

$$\tilde{u}^* \to a^*(k,t) \quad \text{as} \quad \eta \to 1, \qquad \tilde{p}^* = |k|\,a^*, \tag{3.10b, c}$$

$$\tilde{u}^* = \tilde{v}^* = 0 \quad \text{on} \quad \eta = 0, \qquad \tilde{v}^* = -\mathrm{i}k \int_0^\eta \tilde{u}^* f'(\zeta)\,\mathrm{d}\zeta, \tag{3.10d, e}$$

where

$$R_1^* = \mathrm{i}k\tilde{U}_Y^*\,\tilde{u}_0 + \tilde{V}^*\tilde{u}_{0YY}, \quad R_2^* = (\tilde{U}\tilde{u}_{XY} + \tilde{U}_{XY}\,\tilde{u} + \tilde{v}\tilde{U}_{YY} + \tilde{V}\tilde{u}_{YY})^*, \tag{3.10f, g}$$

$\tilde{U}$, $\tilde{V}$ are the steady-flow perturbations to the Blasius flow from the fully nonlinear steady problem, and

$$\tilde{u} = \int_0^\eta \tilde{\tau}^*(k, \eta, t) f'(\xi)\, \mathrm{d}\xi. \tag{3.10h}$$

Next, we combine the outer boundary condition (3.10b), the interaction law (3.10c) and the momentum equation (2.6) evaluated at $Y = 0$ to give the condition

$$\frac{\tilde{\tau}^*_\eta(k, 0, t)}{f'(0)} = \mathrm{i}k|k| \left[\int_0^\eta f'(\xi)\, \tilde{\tau}^*(k, \xi, t)\, \mathrm{d}\xi \right]_{\eta \to 1}. \tag{3.11}$$

To solve the problem we first evaluate $\tilde{U}$ and $\tilde{V}$ using the spectral method described in Burggraf & Duck (1981), suitably modified for the non-uniform Y-grid discussed above. We then solve (3.10) using two different spectral methods. The first is a time-marching scheme similar to the one used in Duck (1985), while the second method incorporates the time periodicity of the solution into the scheme solving the subsequent quasi-steady problem as in the finite-difference approach.

3.3.1. *Time-marching spectral method*

We use a Crank–Nicolson time-marching scheme evaluating R_2^* in physical space with iteration at each time step. Since $\tilde{\tau}$ is a real function

$$\tilde{\tau}^*(k, \eta, t) = \text{c.c.}\{\tilde{\tau}^*(-k, \eta, t)\}, \tag{3.12}$$

where c.c. denotes the complex conjugate, we can truncate the doubly infinite k-range and solve for $k_{\min} \leqslant k \leqslant 0$ and use (3.12) to find $\tilde{\tau}^*$ for $0 < k \leqslant k_{\max}$.

We discretize the (k, η, t)-domain into a uniformly spaced grid solving for $\tilde{\tau}^*$ at the grid points at times

$$t = t_{\min} + (\mathrm{i} - 1)\, \Delta t, \quad \mathrm{i} = 1, 2, \ldots.$$

Equation (3.10) is approximated at $(k, \eta, t - \frac{1}{2}\Delta t)$ by (3.21) in Duck (1985) where $\beta^{-2} = S_0$ and

$$R^*(k, \eta, t - \tfrac{1}{2}\Delta t) = -R_1^*(k, \eta, t - \tfrac{1}{2}\Delta t) - \tfrac{1}{2}[R_2^*(k, \eta, t) + R_2^*(k, \eta, t - \Delta t)]. \tag{3.13}$$

We also approximate (3.11) at time t by using trapezoidal quadrature for the integral and three-point backward differencing for the derivative term. At time t we calculate R_1^* and use $\tilde{\tau}^*(k, \eta, t - \Delta t)$ as the first guess for $\tilde{\tau}^*(k, \eta, t)$ for the calculation of $R_2^*(t)$. For each value of k we solve the set of equations (3.13) by Gaussian elimination, a process which results in a tridiagonal system with a full bottom row. Next we calculate R_2^* by inverting spectral variables into physical space (using the fast Fourier transform (FFT) method of Cooley & Tukey 1965) then calculating R_2, followed by transformation of R_2 to R_2^* using the FFT routine again. Finally, we then solve the tridiagonal system for each k with the updated values of R_2^*. Iteration continues until the maximum change in the spectral pressures between iterations is less than some prescribed tolerance (typically 10^{-6}). The scheme then steps forward to the next time step and repeats the iteration process.

At $t = t_{\min}$, the start-up time, we solve (3.10) evaluated at $(k, \eta, t_{\min})$ with the time-derivative term removed. This method is found to give a smoother start dominated less by transients than a purely impulsive start (see Duck 1988).

3.3.2. *Time-periodic spectral method*

In this method we write

$$\tilde{u}_0 = \mathrm{Re}\{\hat{u}_1(Y)\,\mathrm{e}^{-\mathrm{i}t}\}, \quad \tilde{\tau} = \mathrm{Re}\{\tilde{\tau}_1(X, Y)\,\mathrm{e}^{-\mathrm{i}t}\}, \tag{3.14a, b}$$

and let an asterisk denote the Fourier transform of some quantity; then (3.10) becomes

$$-\mathrm{i}S_0\tilde{\tau}_1^* + \mathrm{i}kf(\eta)\,\tilde{\tau}_1^* - (f')^{-2}\tilde{\tau}_{1\eta\eta}^* + (f')^{-3}f''\tilde{\tau}_{1\eta}^* = -(\mathrm{i}k\tilde{U}_Y^*\hat{u}_1 + \tilde{V}^*\hat{u}_{1YY}) - (\tilde{U}\tilde{u}_{1XY} + \tilde{U}_{XY}\hat{u}_1 + \tilde{v}_1\tilde{U}_{YY} + \tilde{V}\tilde{u}_{1YY})^*. \tag{3.15}$$

The numerical solution of (3.15) is similar to the solution of the steady problem. We then use (3.14) to find the solution at any time t. For this method $\tilde{\tau}(X, Y)$ is complex valued and (3.12) no longer holds so we must solve the spectral equations over the entire k-range. Obviously there are no problems with transients since (3.15) is a quasi-steady problem. Unfortunately, this approach is only suitable for subcritical values of S_0 because as S_0 increases from subcritical to supercritical values one of the poles of $\tilde{\tau}^*$ migrates from the upper half-plane of k-space to the lower half-plane (Duck 1985). This pole should be included in the physical $X > 0$ solution by deforming the Fourier inversion contour. The time-periodic method would wrongly include the contribution of this pole in the $X < 0$ solution. In principle we could treat this problem for supercritical S_0 by solving the spectral equations in complex k-space, but this would be a formidable numerical task.

4. Numerical results

In this section the results of the numerical computations using both the finite-difference and spectral methods will be presented. In the figures that follow, the finite-difference results are represented by solid curves and the spectral results by circles.

We first consider the effect of the Strouhal number S_0 on the interaction between the unsteady flow and the surface distortion. To minimize any nonlinear effects, a small value of the hump height, $h = 0.1$, for which separation does not occur in the mean flow, was chosen. The numerical solution was found for several values of S_0, ranging from 0.5 to 3.5. For the finite-difference method, in most cases 200 points were taken in the streamwise direction over the range $-10 \leqslant X \leqslant 10$ ($\Delta X = 0.10$). To solve the lower-deck equations, 50 points were taken across the lower-deck region over the range $0 \leqslant Y \leqslant 7.5$. Also, an additional 50 points were used in the upper-deck $\hat{y}$ scaling over the range $0 \leqslant \hat{y} \leqslant 5$, to solve Laplace's equation for the pressure in the upper-deck region. To test the sensitivity of the thickness of the upper-deck region, in some cases the upper-deck range was extended to $\hat{y} = 10$ (100 points), but no significant differences in the results were noticed. For the time-marching spectral method a typical spectral space grid used for the calculations was 256×25 points over the range approximately $-10 \leqslant k \leqslant 0$ and $0 \leqslant \eta \leqslant 0.95$ with a time step $\Delta t = 0.005$, this corresponding to a physical grid with $\Delta X = 0.314$ and $-80.4 \leqslant X \leqslant 80.1$, approximately. Finally, a typical grid used for the time-periodic spectral method was 512×25 over the range approximately $-10 \leqslant k \leqslant 10$ and $0 \leqslant \eta \leqslant 0.95$. Note that the fast Fourier transform used by the spectral methods required a slight bias in the k-range, namely $k_{\min} \leqslant k \leqslant -k_{\min} - \Delta k$ (see Burggraf & Duck 1981). Results from

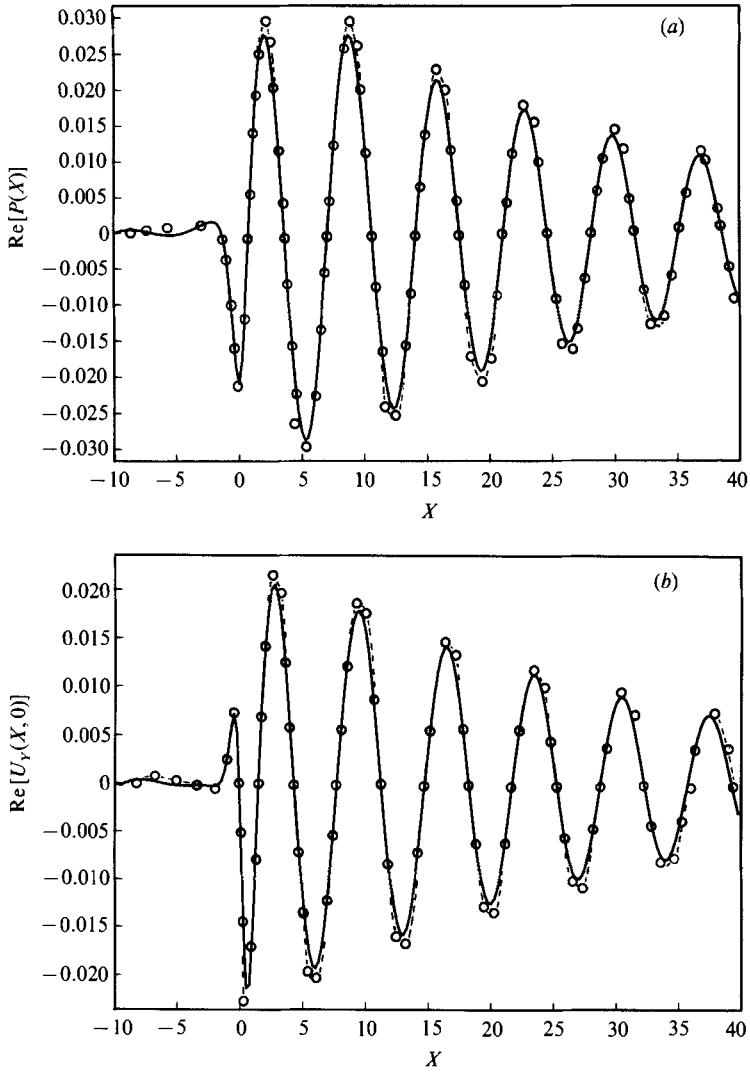

FIGURE 3. (*a*) Disturbance pressure, (*b*) disturbance wall shear, for $S_0 = 2$, $h = 0.1$. ——, finite-difference method; ○, spectral method.

both spectral methods were checked using grids with double the number of points in the η-direction, grids with more extensive k-ranges, and grids with a finer mesh size, giving graphically indistinguishable results.

Using the finite-difference method of solution, convergence of the numerical computations was achieved when the absolute value of the difference in the displacement thickness $-a(X)$ between two successive iterates was less than 10^{-5} for all X. The number of iterations required for convergence was found to be quite sensitive to the value of S_0 under consideration and also to the initial guesses taken for the disturbance profiles. For a subcritical disturbance of $S_0 = 0.5$, less than 100 iterations were sufficient for convergence. However, for a supercritical disturbance with $S_0 = 3.0$ approximately 3400 iterations were necessary to obtain converged results. Also, by gradually increasing the value of S_0 and using the converged

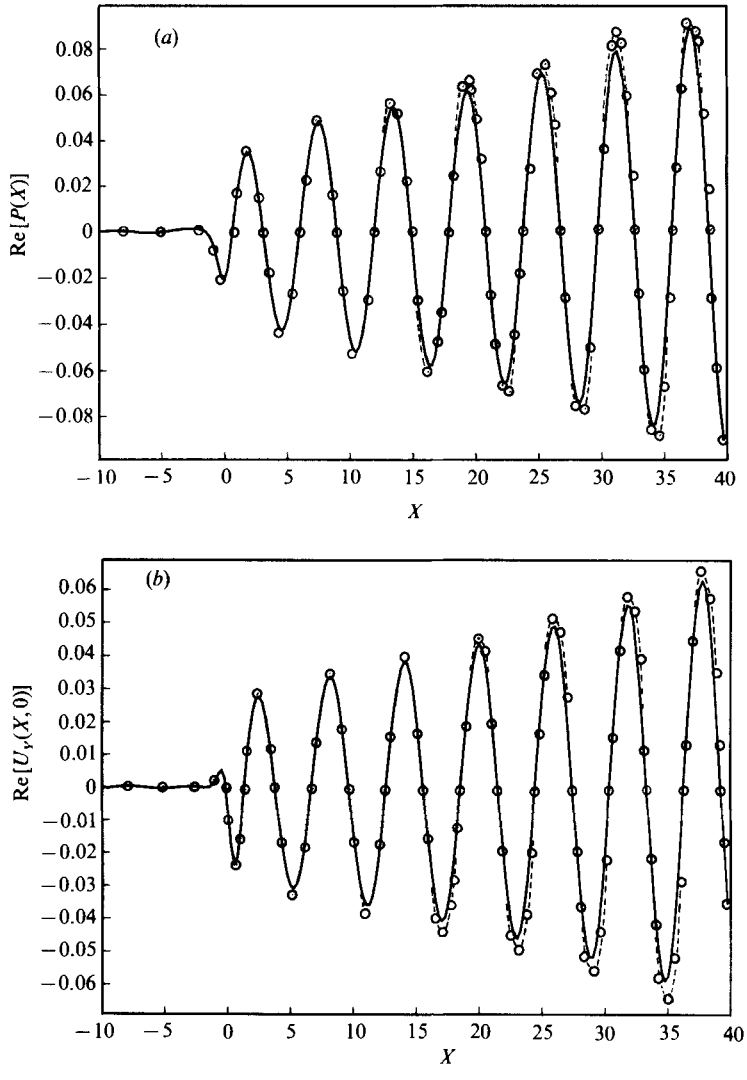

FIGURE 4. (*a*) Disturbance pressure, (*b*) disturbance wall shear, for $S_0 = 2.5$, $h = 0.1$. ——, finite-difference method; ○, spectral method.

solution for the previous value of S_0 as the initial guess, we could reduce the number of iterations required and also maintain a small maximum fluctuation between successive iterative values of the displacement thickness.

The disturbance produced by the interaction with the hump should ultimately decay sufficiently far downstream of the hump if the scaled free-stream Strouhal number is below its critical value $S_{0_{\text{crit}}} \approx 2.296$. To illustrate this eventual damping of the unsteady disturbances, an extended range of $-10 \leqslant X \leqslant 40$ ($\Delta X = 0.25$) was considered. The real parts of the complex-valued disturbance pressure and wall shear distributions for a representative subcritical case, $S_0 = 2$, are presented in figure 3 using both the finite-difference and spectral methods. The decay in the disturbance amplitude for all quantities is clearly seen for $X \geqslant 10$. Similarly, the disturbances should amplify downstream of the surface distortion if S_0 is supercritical. The same

extended X-range was thus considered for a typical supercritical case, $S_0 = 2.5$, and figure 4 shows the amplification of the disturbances in the streamwise direction in this case.

For the subcritical case the spectral method results presented here were computed using the time-periodic spectral method on a grid sufficiently fine and extensive to give grid-independent results. The supercritical results given in figure 4 were calculated using a linearized time-marching scheme and are shown for $t = 14\pi$. For both cases, excellent agreement exists between the finite-difference and spectral method results for the positioning of the T–S waves. There is a discrepancy of approximately 10% in the wave amplitudes. This difference can be reduced by increasing the number of grid points in the X-direction of the finite-difference method, as discussed below.

Numerical experiments using the finite-difference method indicate that we can enhance the convergence rate in subcritical cases by extending the X-domain. The further downstream we place the boundary, the more the disturbance is damped near the boundary and this, in turn, speeds up the global convergence properties of the scheme. Conversely, for supercritical disturbances the further away the downstream boundary is placed, the larger the value of the disturbance amplitude becomes, and this results in a further increase in the number of iterations required for convergence.

We next consider the nonlinear problem with a hump height of $h = 1.0$. In this case the mean flow is still attached everywhere in the flow field. The disturbance solution for this case has the same shape and follows the same pattern as the previous solutions for $h = 0.1$ over the entire range of Strouhal numbers considered in this study. However, now the amplitudes of the disturbances are increased by a factor of approximately 10, which indicates a linear mechanism for the amplification of the disturbances due to increasing the height, at least for this range of values of h.

The growth rate k_i and the wavelength λ of the T–S waves can be calculated from the numerical results and compared with the values given by the analytical theory (Duck 1985). The pressure

$$\tilde{p}(X,t) = \mathrm{Re}\{\tilde{p}_1(X)\,\mathrm{e}^{-\mathrm{i}t}\},$$

where $\tilde{p}_1(X)$ is calculated using the time-periodic spectral method. Now $\tilde{p}_1(X) = C\,\mathrm{e}^{\mathrm{i}kX}$ + a function of X which decays algebraically as $X \to \infty$, and C is a constant. Therefore,

$$\frac{\mathrm{d}\tilde{p}_1/\mathrm{d}X}{\tilde{p}_1} \approx \mathrm{i}k, \quad \frac{\mathrm{d}^2\tilde{p}_1/\mathrm{d}X^2}{\tilde{p}_1} \approx -k^2,$$

where $k = k_r + \mathrm{i}k_i$ and $\lambda = 2\pi/k_r$. This approximate method for calculating k should become more accurate when k is calculated from higher-order derivatives of the pressure. Figure 5 (a, b) shows the values obtained at each X station for the linearized time-periodic spectral results for the case $S_0 = 1.0$ calculated from the second derivative of the pressure. For comparison purposes, the finite-difference results for k calculated using the first-derivative approximation for the pressure are also shown. The two methods give substantially the same results for $X > 10$. In the region $12 < X < 40$ the values of k_r are within 3% of the analytical value of $k_r \approx -0.522$ and the values of k_i within about 10% of $k_i \approx 0.121$. The reason for the larger percentage error in k_i compared to k_r is that $|k_i| < |k_r|$. As is to be expected, as we move upstream of this region the algebraic terms become significant as the influence of the hump increases and the calculated values of k_r, k_i show greater variation from their analytical values.

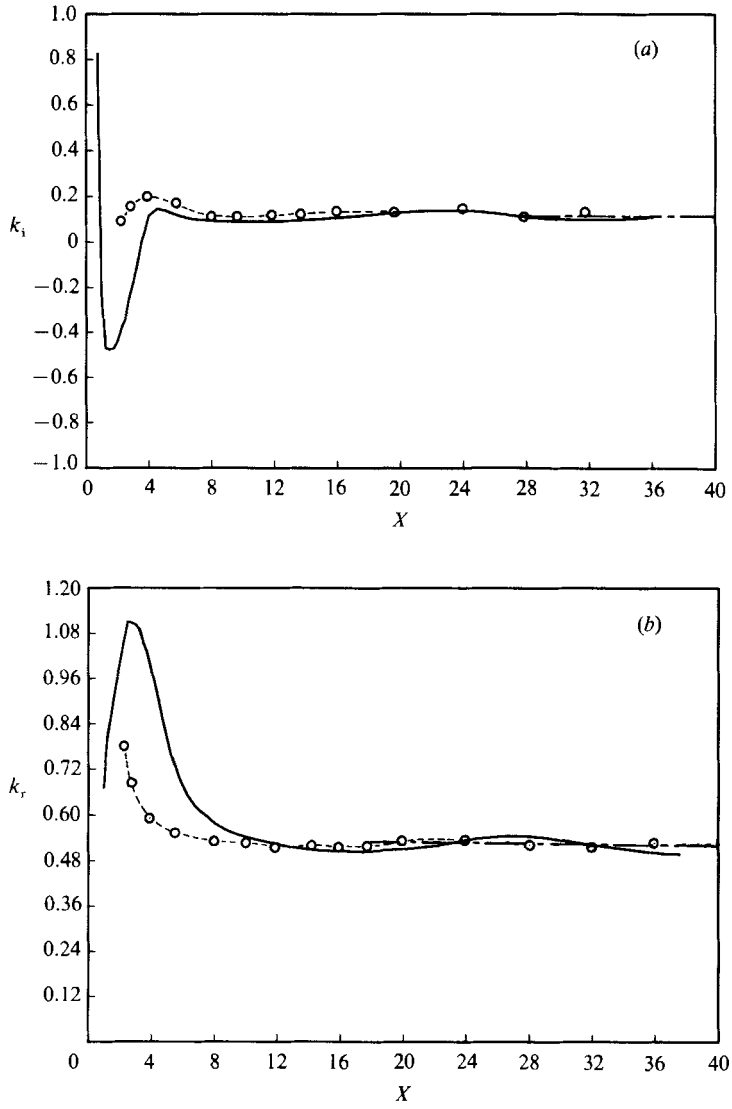

FIGURE 5. (*a*) Tollmien–Schlichting wave growth rate, (*b*) Tollmien–Schlichting wavelength; ——, finite-difference method; ○, spectral method; – – – – –, analytical value.

Figure 6 shows the results obtained for $h = 1.0, S_0 = 3$. The finite-difference results were calculated using an X-grid of $-10 \leqslant X \leqslant 10$ with $\Delta X = 0.125$. The time-marching spectral method results here are for $t = 5\pi$ (with the negative of the results plotted for comparison with the finite-difference solution). By this time the time-periodic solution is established in the region approximately $X < 13$ and here there is excellent agreement with the finite-difference results.

For $h = 1.0$ the results for a typical subcritical value of S_0, namely $S_0 = 1$, were calculated using both the time-marching spectral method and the time-periodic method. The start-up of the time-marching method generated unstable modes in the form of transients which were propagated downstream. The triggered unstable mode transients led to extremely rapid, large-amplitude oscillations in the spectral space

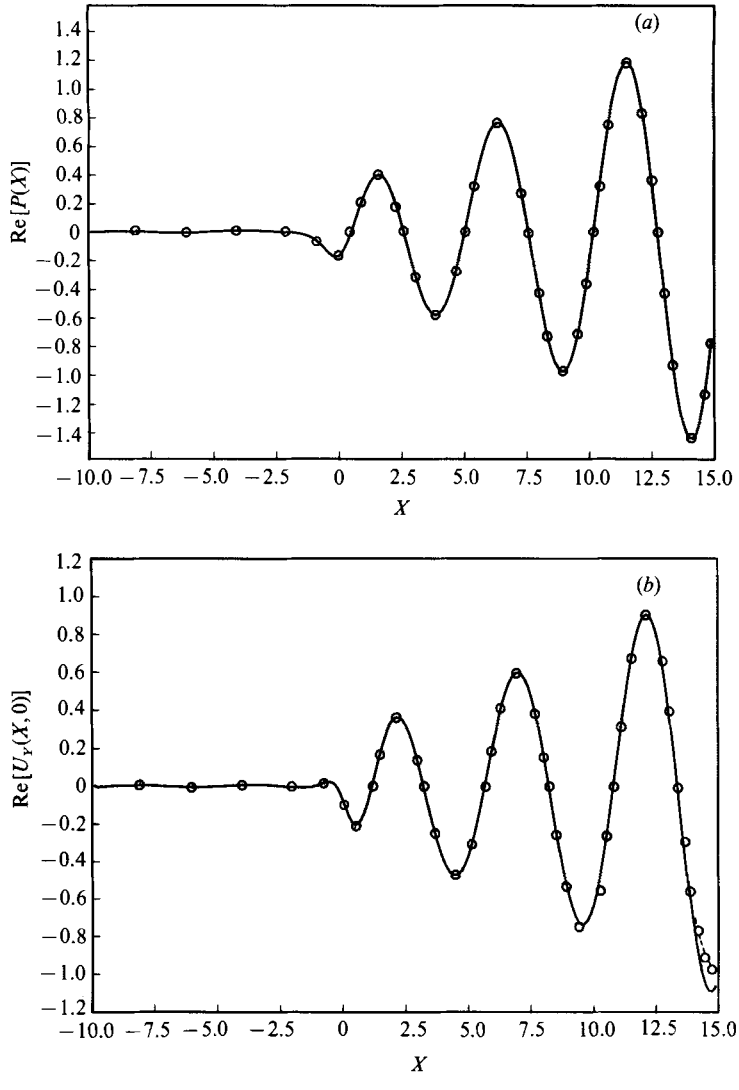

FIGURE 6. (*a*) Disturbance pressure, (*b*) disturbance wall shear, for $S_0 = 3$, $h = 1$. ——, finite-difference method; ○, spectral method.

solution and the scheme failed when they became too rapid to be correctly described by the grid, giving spurious upstream oscillations in the physical solution. The time-periodic solution established itself increasingly further downstream as time progressed; for example, for $h = 1$, $S_0 = 1$, it extended over the region $X < 14$ by time $t = 2\pi$. Using a grid of 256×25 over the approximate range $-10 \leqslant k \leqslant 10$, $0 \leqslant \eta \leqslant 0.95$ with a time step of $\Delta t = 0.005$ and $t_{\min} = -\frac{1}{2}\pi$ it took approximately 3000 s Cyber 205 c.p.u. time. For the same problem the time-periodic method took 8 iterations to converge and approximately 40 s Cyber 205 c.p.u. time using a grid of 1024×25 for $-10 \leqslant k \leqslant 10$. It was found that the time-periodic solutions obtained using both spectral methods were graphically indistinguishable.

Next, results for $h = 5$, for which the mean flow has a small region of separated flow, are presented. In figure 2, the corresponding mean flow distributions for the

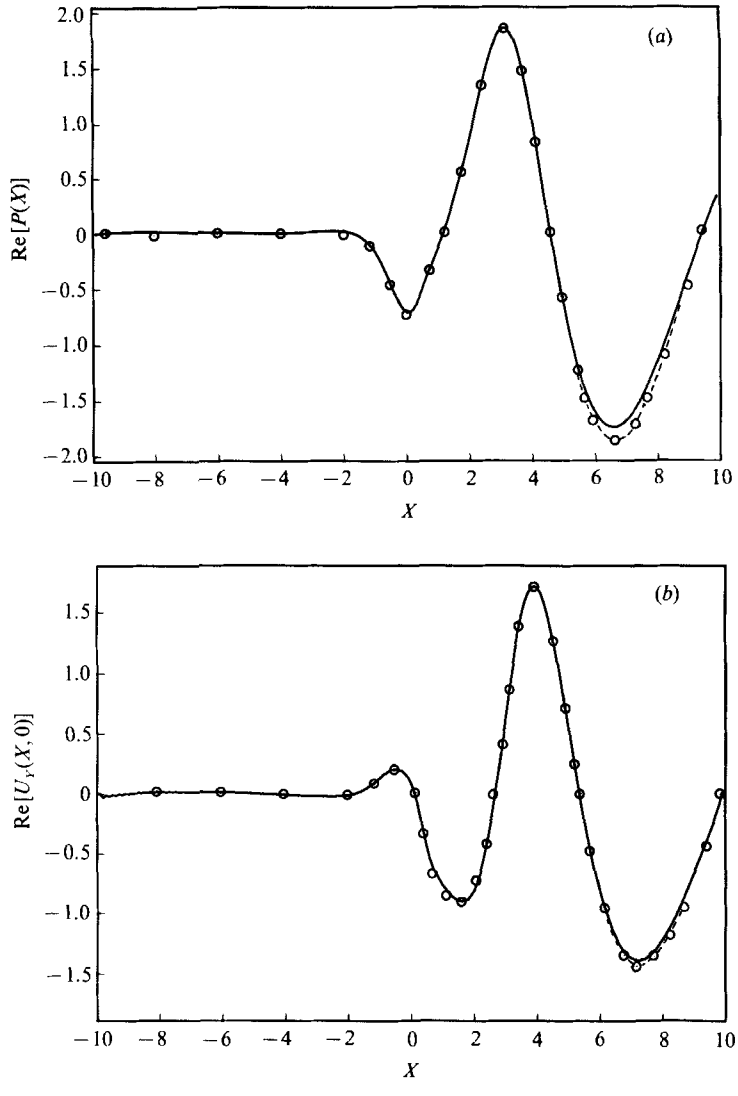

FIGURE 7. (a) Disturbance pressure, (b) disturbance wall shear, for $S_0 = 1$, $h = 5$. ——, finite-difference method; ○, spectral method.

pressure and wall shear are presented. We note that the solutions obtained by the finite-difference method and the steady spectral method are in excellent agreement. There are some small oscillations in the wall shear results in the reversed-flow region, suggesting the need for a somewhat finer grid for the finite-difference method. This effect was confirmed by running the finite-difference code on a somewhat finer grid ($-10 \leqslant X \leqslant 10$, 400 points). In this case the oscillations noted above did indeed disappear.

For this value of h, the finite-difference method was used to obtain converged solutions for $S_0 = 1$ and 1.2. Pressure and wall shear distributions for the unsteady flow over the X-domain $-10 \leqslant X \leqslant 10$ are given in figure 7 for $S_0 = 1$.

Converged solutions using the finite-difference method for larger values of the

Strouhal number are possible in principle; however, the computer time necessary to achieve them becomes prohibitive. Furthermore, the accuracy of the numerical solutions deteriorates as the streamwise step size, ΔX, is increased. This deterioration can best be seen in the wall shear results. Maintaining the same number of mesh points (200) and increasing ΔX we have been able to find three other 'numerically converged' solutions for $h = 5$ and $S_0 = 1$. The wall shear distributions for these solutions are given in figure 8. Note that for all cases the general shape of the solutions do not change. However, by increasing ΔX the magnitude of the disturbance amplitude was reduced while maintaining its same form and location. For the largest value of ΔX, which corresponds to an X-domain of $-10 \leqslant X \leqslant 90$ ($\Delta X = 0.50$), the numerical breakdown is clearly seen in figure 8(*c*) even though the general shape of the distribution has not changed appreciably. For this same X-domain, another 'numerical solution' was obtained for half the step size by doubling the number of points to 400 and the results are shown in figure 8(*d*). Note that the numerical oscillations have disappeared and the same general shape of the curve remains. However, the magnitude of the amplitude is the same as that in figure 8(*b*). There thus seems to be a trade-off between a larger X-domain to help the convergence rate and a smaller step size to maintain an accurate solution.

Alternatively, results for all subcritical values of S_0 can easily be found using the time-periodic spectral method. For $h = 5$, $S_0 = 1$, the finite-difference results were calculated on the three grids $-10 \leqslant X \leqslant 40$, $\Delta X = 0.25$; $-10 \leqslant X \leqslant 20$, $\Delta X = 0.15$; and $-10 \leqslant X \leqslant 10$, $\Delta X = 0.1$, giving discrepancies in the amplitude of the T–S wave of up to 30%, 10% and 5%, respectively, when compared with the time-periodic spectral method results which were calculated on a grid sufficiently fine and extensive to give grid-independent results to graphical accuracy. A comparison of these results for the spectral method and the finite-difference method using the third grid is also given in figure 7.

For $h = 5$, we were unable to obtain a time-periodic solution for any value of S_0 using the spectral time-marching method. To investigate this problem we took the time-periodic solution for $h = 5$, $S_0 = 1$ calculated using the time-periodic spectral method and used it as the start-up for the time-marching method. Time marching the solution resulted in a grid-dependent rapid growth in the spectral space solution for $|k| \gg 1$, with the growth being most rapid for the calculations with the smallest time step Δt and on grids with the most extensive k-ranges. We believe that the numerical problems for the time-marching spectral method for $h = 5$ are possibly caused by an inviscid Rayleigh-type instability (Smith & Bodonyi 1985; Tutty & Cowley 1986).

A comparison between the numerical computations and Goldstein's (1985) analytical theory for $h \ll 1$ can also be made. The disturbance amplitude computed by these two methods is shown in figures 9(*a*) and 9(*b*) for $h = 1$, $S_0 = 3$ and $h = 5$, $S_0 = 1.2$, respectively. For $h = 1$, the analytical theory and the numerical results are in good agreement over most of the region of interest. Smaller values of h and other values of S_0, not shown here, indicate an even better agreement between the two approaches. Thus we can conclude that the analytical theory can be applied for $h < 1$. Conversely, for $h = 5$, the disturbance amplitude predicted by Goldstein's theory does not agree well with that predicted by the numerical computations. The nonlinear base flow results in substantial differences of the receptivity problem from that computed by the analytical theory.

We next consider the physical implications of the numerical results, and in

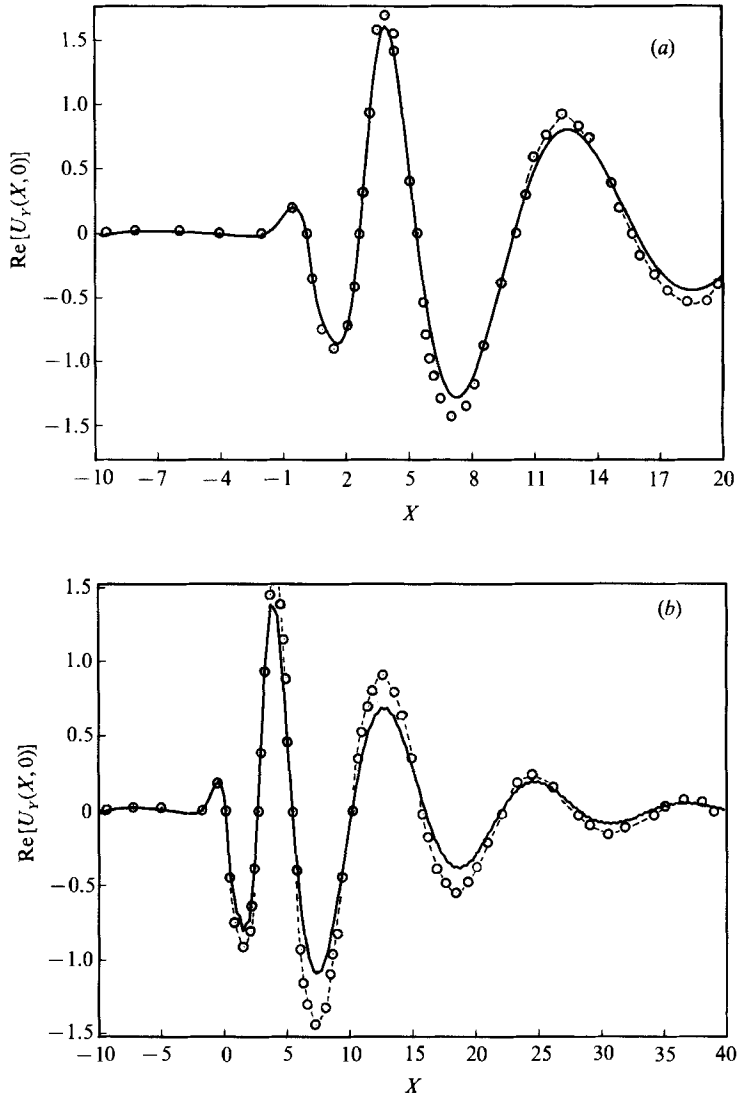

FIGURE 8(*a*, *b*). For caption see facing page.

particular the effect of the hump height h on the disturbance wave amplitude. We choose to follow the amplitude variation with h of several peaks in the disturbance wall shear solution. These peak values are scaled by the corresponding peak values of the linear results, obtained by solving the equations for $h = 1$, setting $R_2^* = 0$ in (3.13) using the time-marching spectral method. Note that the location of the peaks does vary slightly with h. The peak-amplitude dependence on h was studied for subcritical values of S_0, namely $S_0 = 1, 2$, and for the supercritical value $S_0 = 3$. The subcritical solutions were calculated using the time-periodic spectral method, and the supercritical solutions using the time-marching spectral method. The $S_0 = 3$ solutions were found for $h \leqslant 3.5$, calculations for larger values of h were affected by a grid-dependent rapid growth in the spectral plane solution for $|k| \gg 1$. This possible Rayleigh instability is suppressed in the time-periodic spectral method and the finite-

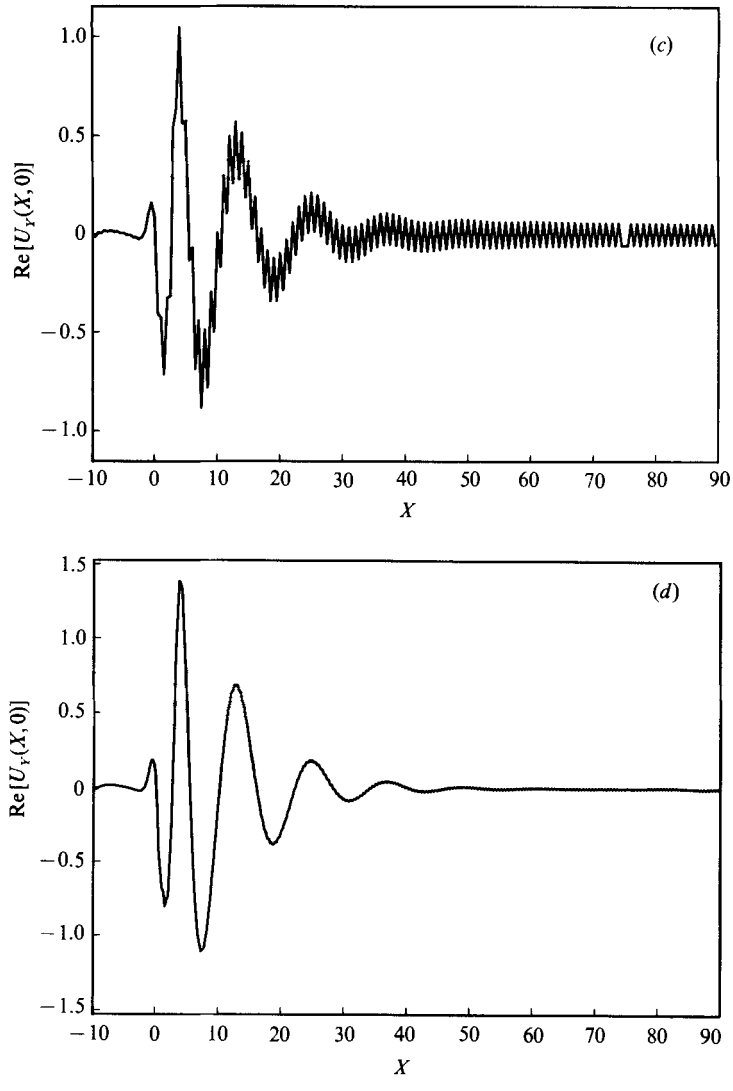

FIGURE 8. Disturbance wall shear for $S_0 = 1$, $h = 5$ and X varying between (*a*) $-10 \leqslant X \leqslant 20$, (*b*) $-10 \leqslant X \leqslant 40$. ——, finite-difference method; ○, spectral method; (*c*) $-10 \leqslant X \leqslant 90$ with $\Delta X = 0.50$, (*d*) $-10 \leqslant X \leqslant 90$ with $\Delta X = 0.25$.

difference method which treats the 'steady-state' equations to find solutions which are periodic in time. Consequently, solutions can be found for $1 \leqslant h \leqslant 5$.

In figures 10(*a*) and 10(*b*) we show the results for $S_0 = 1$ and $S_0 = 3$, giving the scaled peak-amplitude behaviour for the wall shear $\tilde{\tau}(x, 0)$ with h for two different peaks; the results for $S_0 = 2$, not presented here, follow a similar pattern.

For $h < 1$, the scaled disturbance amplitude depends approximately linearly on the hump height. Experimentally, Azin & Polyakov (1979) found a linear dependence of the disturbance amplitude on h, for the interaction of upstream-propagating sound waves with thin mylar strips fixed on a flat plate near the lower branch of the neutral stability curve. For larger values of h, our results show an increasingly

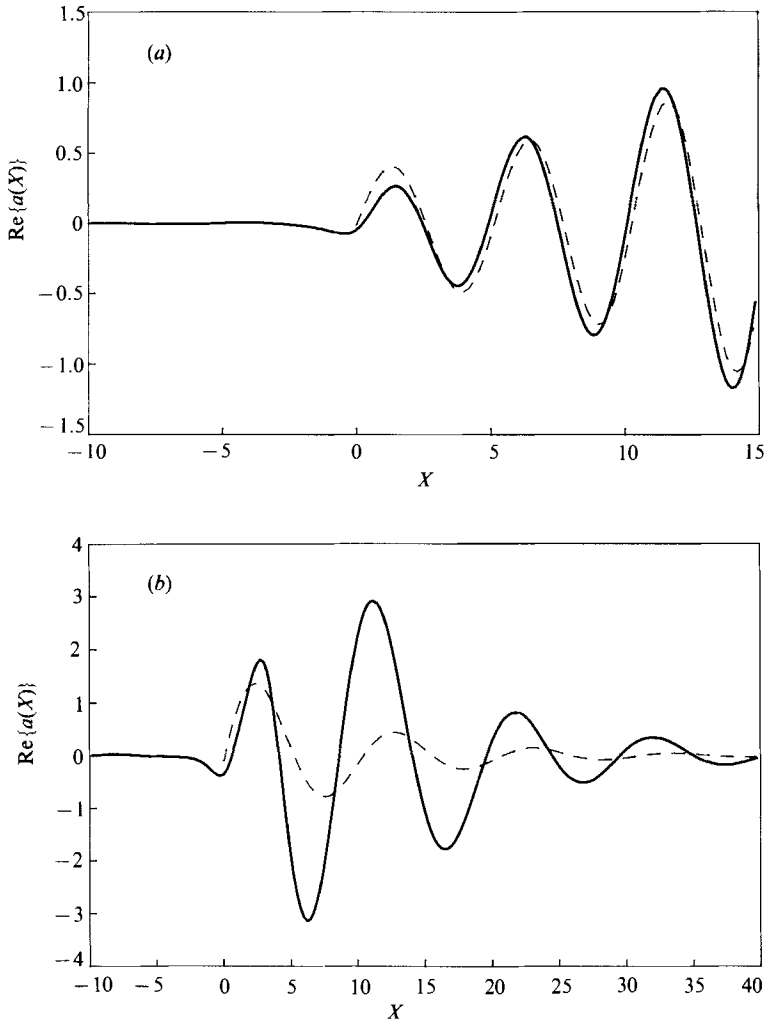

FIGURE 9. Comparison of disturbance displacement distribution for (a) $h = 1$, $S_0 = 3$, and (b) $h = 5$, $S_0 = 1.2$. ——, finite-difference method; – – –, analytical theory.

nonlinear enhancing effect on the disturbance amplitude. These results are confirmed by the finite-difference results for $S_0 = 1$. For example, for $h = 3$ the disturbance amplitude is approximately twice that of the linear results for the same h. The results for the subcritical S_0 calculated using the time-periodic spectral method and finite-difference method show that this increasingly rapid enhancement of the 'receptivity' continues for $h = 4$ and 5. The results for $h = 4, 5$ are approximately three and six times, respectively, the corresponding linear results for the same h.

In conclusion we find a linear dependence of the disturbance amplitude on the hump height for sufficiently small values of h. For moderate $h (1 \leqslant h \leqslant 3)$ we find an enhancement of the receptivity by the nonlinear effect of hump height. For large h where local flow separation can occur in the steady flow, we find a possible short-wavelength instability in our time-marching calculations and a rapidly increasing enhanced receptivity in our 'steady-state' calculations.

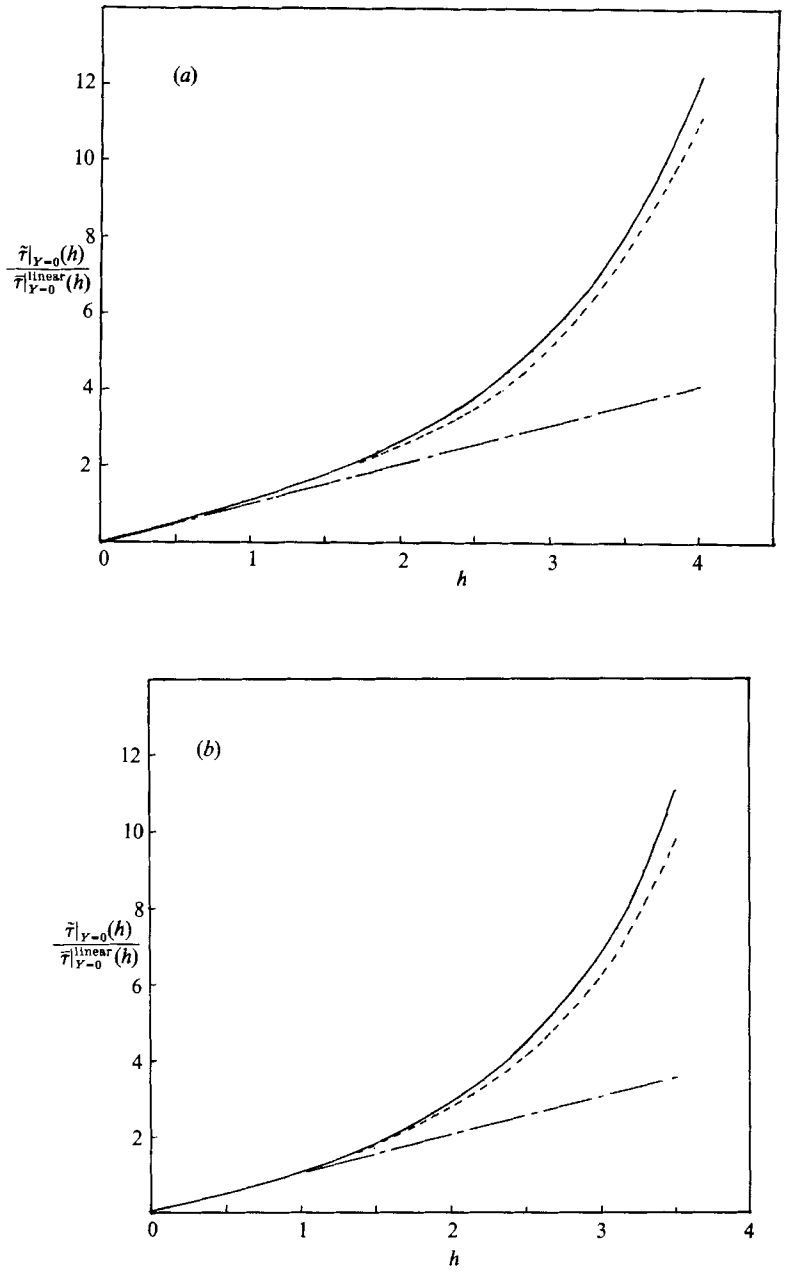

FIGURE 10. (*a*) Disturbance amplitude variation versus h for $S_0 = 1$, normalized by the linearized results for $h = 1$, $S_0 = 1$. ——, minimum near $X = 18.5$; – – –, peak near $X = 13$; — — —, linear result. (*b*) Disturbance amplitude variation versus h for $S_0 = 3$, normalized by the linearized results for $h = 1$, $S_0 = 3$. ——, minimum near $X = 9$; – – –, peak near $X = 7$; — — —, linear result.

R.J.B. is grateful to the National Aeronautics and Space Administration which sponsored the research described here under grant NASA NAG 3-743 and to the Ohio Supercomputer Center for providing computer time on the Cray X-MP supercomputer. Likewise, W.J.C.W. acknowledges the receipt of an SERC Studentship. Also, a number of the calculations carried out as part of this research were performed using computer resources provided by the SERC, grant GR/E/25702. R.J.B. would like to acknowledge Professor F. T. Smith for originally suggesting the problem under study here. Finally, the authors would like to acknowledge Professor O. R. Burggraf for suggesting the use of the radiation condition as the downstream boundary condition for the finite-difference calculations.

REFERENCES

AIZIN, L. B. & POLYAKOV, N. F. 1979 (in Russian) *Preprint 17, Akad. Nauk USSR, Siberian Div., Inst. Theor. Appl. Mech., Novosibirsk.* (See also Nishioka, M. & Morkovin, M. V. 1986 *J. Fluid Mech.* **171**, 219).

BODONYI, R. J. & DUCK, P. W. 1988 *Computers Fluids* **16**, 279.

BODONYI, R. J., SMITH, F. T. & GAJJAR, J. 1983 *IMA J. Appl. Maths* **30**, 1.

BURGGRAF, O. R. & DUCK, P. W. 1981 In *Numerical and Physical Aspects of Aerodynamic Flows* (ed. T. Cebeci). Springer.

COOLEY, J. W. & TUKEY, J. W. 1965 *Math. Comp.* **19**, 297.

DUCK, P. W. 1984 *Q. J. Mech. Appl. Maths* **37**, 57.

DUCK, P. W. 1985 *J. Fluid Mech.* **160**, 465.

DUCK, P. W. 1988 *J. Fluid Mech.* **197**, 254.

DUCK, P. W. 1989 *Computers Fluids* (to appear).

DUCK, P. W. & BURGGRAF, O. R. 1986 *J. Fluid Mech.* **162**, 1.

GEDNEY, C. J. 1983 *Phys. Fluids* **26**, 1158.

GOLDSTEIN, M. E. 1983 *J. Fluid Mech.* **127**, 59.

GOLDSTEIN, M. E. 1984 *J. Fluid Mech.* **145**, 71.

GOLDSTEIN, M. E. 1985 *J. Fluid Mech.* **154**, 509.

GOLDSTEIN, M. E. & HULTGREN, L. S. 1987 *J. Fluid Mech.* **181**, 519.

GOLDSTEIN, M. E., LEIB, S. J. & COWLEY, S. J. 1987 *J. Fluid Mech.* **181**, 485.

GOLDSTEIN, M. E., SOCKOL, P. M. & SANZ, J. 1983 *J. Fluid Mech.* **129**, 443.

LEEHEY, P. & SHAPIRO, P. 1979 In *Laminar-Turbulent Transition* (ed. R. Eppler & H. Fasel), p. 321. Springer.

MORKOVIN, M. V. 1969 *Rep.* AFFDL-TR-68-149. Air Force Flight Dyn. Lab, Wright-Paterson AFB, Ohio.

MURDOCK, J. W. 1980 *Proc. R. Soc. Lond.* A **372**, 517.

RESHOTKO, E. 1976 In *Ann. Rev. Fluid Mech.* **8**, 311.

SMITH, F. T. 1973 *J. Fluid Mech.* **57**, 803.

SMITH, F. T. 1985 *Rept.* UTRC85-36, United Technologies Research Center.

SMITH, F. T. & BODONYI, R. J. 1982 *J. Fluid Mech.* **118**, 165.

SMITH, F. T. & BODONYI, R. J. 1985 *Aeronaut. J.* **89**, 205.

SMITH, F. T. & BODONYI, R. J. 1987 *Stud. Appl. Maths* **77**, 129.

SMITH, F. T., BRIGHTON, P. W. M., JACKSON, P. S. & HUNT, J. C. R. 1981 *J. Fluid Mech.* **113**, 123.

SMITH, F. T. & BURGGRAF, O. R. 1985 *Proc. R. Soc. Lond.* A **399**, 25.

STEWARTSON, K. 1969 *Mathematika* **16**, 106.

STEWARTSON, K. 1970 *Q. J. Mech. Appl. Maths* **23**, 137.

STEWARTSON, K. 1971 *Q. J. Mech. Appl. Maths* **24**, 387.

TUTTY, O. R. & COWLEY, S. J. 1986 *J. Fluid Mech.* **168**, 431.

VELDMAN, A. E. P. 1979 *Rep.* NLR-TR-79023. Dutch Nat. Aerosp. Lab., the Netherlands.